Macromolecules

pubs.acs.org/Macromolecules Article

Topologically Induced Heterogeneity in Gradient Copolymer Brush Particle Materials

Yuqi Zhao,[§] Zongyu Wang,[§] Chenxi Yu, Hanshu Wu, Mateusz Olszewski, Rongguan Yin, Yue Zhai, Tong Liu, Amy Coronado, Krzysztof Matyjaszewski,* and Michael R. Bockstaller*

Cite This: *Macromolecules* 2022, 55, 8846–8856 Read Online

ACCESS | Metrics & More | Article Recommendations | Supporting Information

Downloaded via CARNEGIE MELLON UNIV on March 14, 2023 at 15:14:08 (UTC).
See https://pubs.acs.org/sharingguidelines for options on how to legitimately share published articles.

ABSTRACT: A facile synthetic route toward silica brush particles with random and gradient copolymer grafts comprised of *n*-butyl acrylate (BA) and methyl methacrylate (MMA) using surface-initiated atom transfer radical polymerization (SI-ATRP) was developed. The effect of chain architecture on the structure and thermomechanical properties of copolymer-tethered brush particle films was investigated and compared to linear copolymer analogues. Random copolymer brush systems displayed a uniform and narrow glass transition, and the dependence of the glass-transition temperature followed a similar trend as for linear copolymers. In contrast, gradient brush materials featured a splitting of the glass-transition temperature with increasing MMA content along with a step-like increase of Young's modulus and a decrease in ductility. The results were interpreted in terms of the effect of brush architecture on the microstructure of films. The results suggested a "molecularly uniform" microstructure in films of the random brush as well as linear random and linear gradient copolymer systems. In contrast, gradient brush systems featured a heterogeneous microstructure in which MMA-rich regions acted as "traps" that reduced chain mobility. The formation of compositional heterogeneity was rationalized by the "prescribed orientation" of gradient copolymer chains near the particle interface that amplified composition fluctuations and hence local segregation of repeat units. The results highlight the need for a better understanding of the role of "geometric constraints" on the physical properties of copolymer brush particle-based hybrid materials and the opportunity for multiple property enhancement by control of segment distribution in addition to the overall composition.

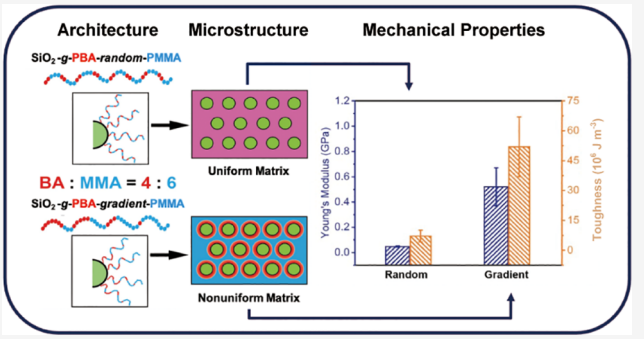

INTRODUCTION

The tethering of polymer chains to the surface of nanoparticles to form "brush particles" (aka "hairy particles") has been shown to provide one-component hybrid materials with improved properties such as biocompatibility, enhanced thermal conductivity, or dielectric breakdown strength that depends on the architecture and composition of the brush particle system.[1−31] Recent advances in the surface-initiated controlled radical polymerization (SI-CRP) significantly expanded the control over structural parameters of surface-bound polymer ligands, such as degree of polymerization, dispersity, or grafting density.[21,32−44] This enabled the synthesis of brush particle systems with structural and dynamical properties that are tunable across the range of soft (polymer-like) to hard (particle-like) interactions.[45,46] Other advantageous features of SI-CRP include the ability to control the chain architecture via the concurrent or sequential reaction of distinct monomers, thus enabling the synthesis of random, gradient, or block copolymer brushes.[47−57] Copolymerization affords new opportunities to design the structure and properties of brush particle-based materials. Elucidation of the structure−property relations in copolymer brush particle systems with varied architecture therefore not only promises new insights into the physics of microstructured colloidal systems but also holds opportunities for the design of hybrid materials with novel functionalities.

To understand the mutual effect of polymer composition and architecture on the properties of brush particle materials, the Young's modulus and the energy absorption during fracture (in the following referred to as "fracture toughness") are of particular interest as they provide information about brush interactions and energy dissipation pathways during small and large strain deformation, respectively. Previous studies have shown that the interaction between brush particles depends on parameters such as the grafting density and degree of polymerization of tethered chains.[24] In the "dense" grafting regime, brush particles were found to interact via hard-sphere

Received: May 31, 2022
Revised: July 17, 2022
Published: July 28, 2022

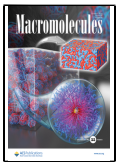

ACS Publications © 2022 American Chemical Society

https://doi.org/10.1021/acs.macromol.2c01131
Macromolecules 2022, 55, 8846−8856

Scheme 1. Illustration of the Synthesis Process of Gradient and Random Copolymer Particle Brushes

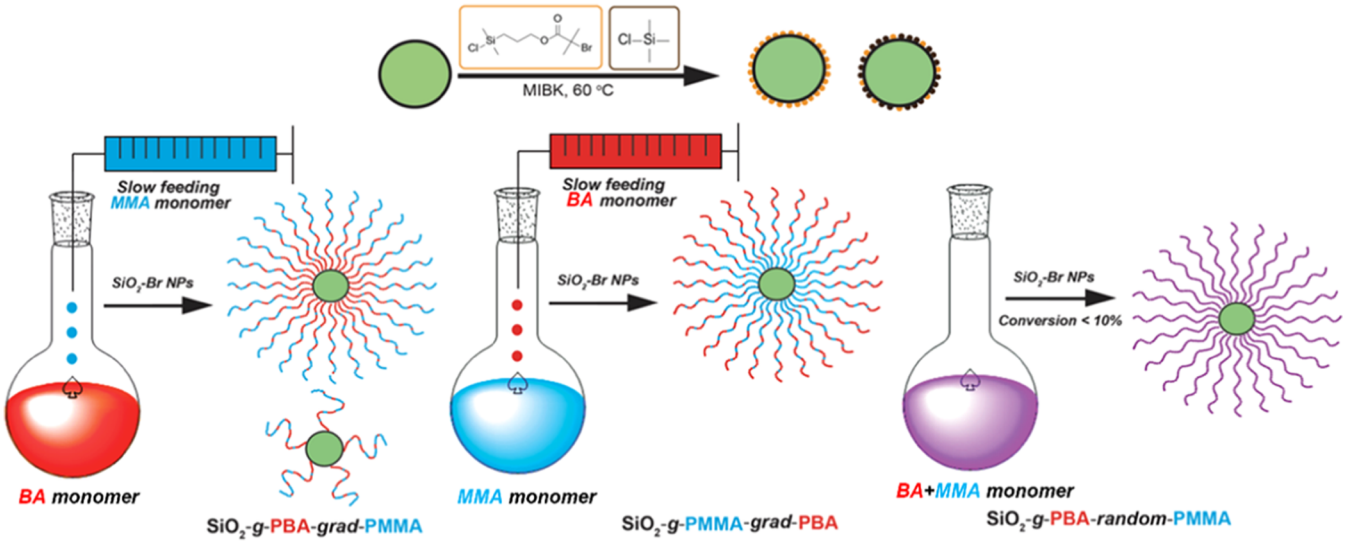

Table 1. Material Characteristics of SiO_2-*g*-PBA-*grad*/*ran*-PMMA Particle Brush Systems

entry[a]	*x*, BA (mol %)[b]	*x*, MMA (mol %)[b]	M_n[c]	M_w/M_n[c]	f_{SiO_2} (%)[d]	σ (nm^2)[e]	T_g (°C)[f]
H-G-B67M33	67.3	32.7	21,040	1.47	20.59	0.61	−20
H-G-B56M44	56.3	43.7	23,150	1.55	21.41	0.53	3
H-G-B50M50	50.4	49.5	36,700	1.37	12.37	0.64	10
H-G-B48M52[g]	48.1	51.9	44,350	1.41	12.96	0.50	−15, 23
H-G-B45M55[g]	45.5	54.5	54,470	1.39	8.94	0.62	−20, 38
H-G-B38M62[g]	38.4	61.6	49,960	1.42	10.14	0.59	−16, 41
L-G-B59M41	58.7	41.3	16,480	1.29	57.19	0.15	−21
L-G-B54M46	54.1	45.9	26,080	1.36	43.95	0.16	0
L-G-B48M52	48.5	51.5	28,210	1.32	51.65	0.11	6
L-G-B44M56[g]	43.6	56.4	32,670	1.37	44.38	0.13	−12, 25
L-G-B39M61[g]	39.1	60.9	44,010	1.36	30.86	0.17	−8, 36
L-G-B33M67[g]	32.8	67.2	36,620	1.43	36.02	0.16	−7, 47
H-G-M25B75	75.0	25.0	28,710	1.38	18.81	0.50	−22
H-G-M46B54	53.8	46.2	38,200	1.30	14.29	0.52	−10
H-G-M50B50	50.1	49.9	29,970	1.29	21.08	0.41	−5
H-G-M57B43	43.5	56.5	37,390	1.33	14.41	0.53	9
H-G-M74B26[g]	26.5	73.5	39,910	1.29	13.76	0.52	−31, 56, 108
H-R-B61M39	61.5	38.5	26,540	1.18	22.13	0.46	−15
H-R-B55M45	54.7	45.3	23,900	1.25	20.81	0.56	−2
H-R-B47M53	46.9	53.1	47,300	1.20	13.71	0.46	9
H-R-B44M56	44.5	55.5	45,420	1.21	13.43	0.49	15
H-R-B38M62	37.6	62.4	50,040	1.16	13.67	0.44	29
R-B46M54	45.6	54.4	58,100	1.34			18
G-B45M55	44.8	55.2	40,270	1.14			16

[a]Reaction conditions: H-G-B_xM_y/L-G-B_xM_y particle brushes: $[BA]_0/[SiO_2\text{-}Br]_0/[CuBr_2]_0/[Me_6TREN]_0/[Sn(EH)_2]_0$ = 5000:1:0.5:5:5 at 50 °C with 25 vol % anisole, V_0(BA) = 15 mL, MMA feeding rate = 0.5/1/1.5/2/2.5/3 mL/h, total [BA]/[MMA] = 5000:1500/3000/4500/6000/7500/9000; H-G-M_xB_y particle brushes: $[MMA]_0/[SiO_2\text{-}Br]_0/[CuBr_2]_0/[Me_6TREN]_0/[Sn(EH)_2]_0$ = 3000:1:0.5:5:5 at 50 °C with 25 vol % anisole, V_0(MMA) = 10 mL, BA feeding rate = 1/1.5/2/2.5/3 mL/h, total [MMA]/[BA] = 3000:3000/4500/6000/7500/9000; H-R-B_xM_y particle brushes: $([BA]_0:[MMA]_0)/[SiO_2\text{-}Br]_0/[CuBr_2]_0/[Me_6TREN]_0/[Sn(EH)_2]_0$= (3300:500)/(4300:1200)/(3000:1000)/(3400:1600)/(2900:1700):1:0.5:5:5 at 50 °C with 30 vol % anisole; G-$B_{45}M_{55}$ linear gradient copolymer: $[BA]_0/[EBiB]_0/[CuBr_2]_0/[Me_6TREN]_0/[Sn(EH)_2]_0$ = 420:1:0.2:2:2 at 50 °C with 10 vol % anisole, V_0(BA) = 3.3 mL, MMA feeding rate = 0.6 mL/h, total [BA]/[MMA] = 420:520; R-$B_{46}M_{54}$ linear random copolymer: $[BA]_0/[MMA]_0/[EBiB]_0/[CuBr_2]_0/[Me_6TREN]_0/[Sn(EH)_2]_0$= 3500:1700:1:0.5:5:5 at 50 °C with 30 vol % anisole. [b]Determined by ^{1}H NMR. [c]Determined by size-exclusion chromatography (SEC). [d]Determined by thermogravimetric analysis (TGA). [e]Calculated by eq S1. [f]The major glass-transition temperature determined by differential scanning calorimetry (DSC). [g]Samples show the multiple "core−shell corona" structures.

type interaction potentials.[58] The avoidance of brush layer interdigitation resulted in brittle behavior of brush particle films.[58] In contrast, more relaxed chain conformations in the limit of low grafting density promoted brush interdigitation and entanglement formation.[59,60] Chain entanglement gave rise to crazing during crack propagation, which increased the fracture toughness of brush particle-based materials.[59,60]

https://doi.org/10.1021/acs.macromol.2c01131
Macromolecules 2022, 55, 8846−8856

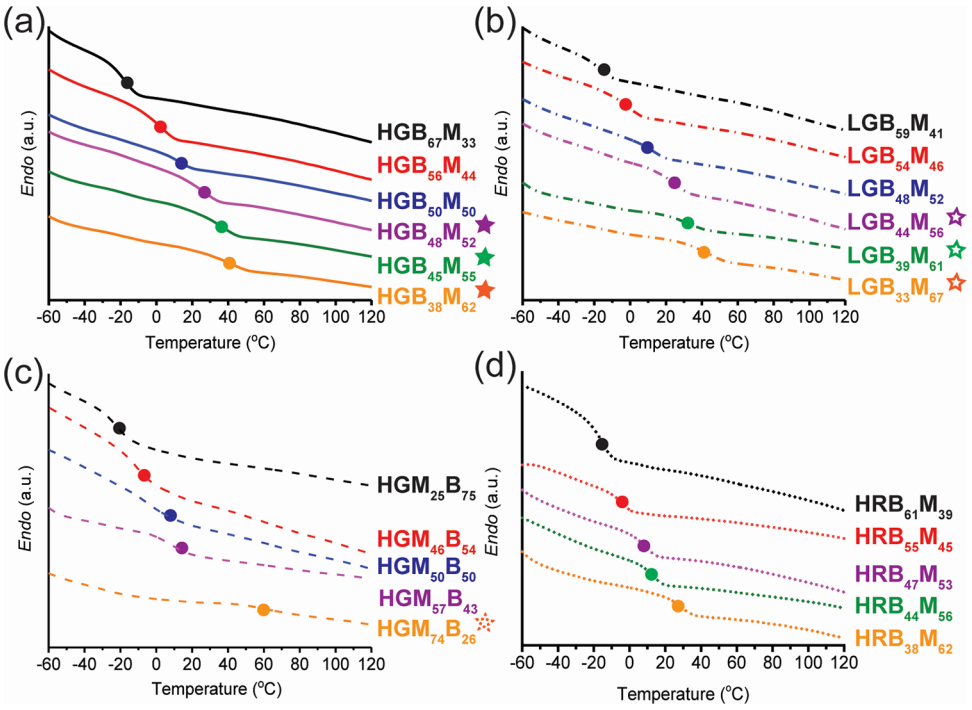

Figure 1. DSC curves for (a), (b) BA-rich inside gradient copolymer particle brushes with high (a) and low (b) grafting density; (c) MMA-rich inside gradient copolymer particle brushes with high grafting density as well as densely grafted random copolymer brush systems (d). The stars in the plots highlight the samples for which multiple T_g's can be distinguished in the respective heat flow derivative curves (Figure 2). The positions of T_g's are highlighted with solid points in the figures. Sample identification is as follows: panel (a)—solid lines, H-G-$B_{67}M_{33}$: black, H-G-$B_{56}M_{44}$: red, H-G-$B_{50}M_{50}$: blue, H-G-$B_{48}M_{52}$: magenta, H-G-$B_{45}M_{55}$: olive, H-G-$B_{38}M_{62}$: orange; panel (b)—dash-dot lines, L-G-$B_{59}M_{41}$: black, L-G-$B_{54}M_{46}$: red, L-G-$B_{48}M_{52}$: blue, L-G-$B_{44}M_{56}$: magenta, L-G-$B_{39}M_{61}$: olive, L-G-$B_{33}M_{67}$: orange; panel (c)—dash lines, H-G-$M_{25}B_{75}$: black, H-G-$M_{46}B_{54}$: red, H-G-$M_{50}B_{50}$: blue, H-G-$M_{57}B_{43}$: magenta, H-G-$M_{74}B_{26}$: orange; and panel (d)—dot lines, H-R-$B_{61}M_{39}$: black, H-R-$B_{55}M_{45}$: red, H-R-$B_{47}M_{53}$: magenta, H-R-$B_{44}M_{56}$: olive, H-R-$B_{38}M_{62}$: orange. All curves were recorded during the third heating/cooling run at a heating rate of 20 °C/min.

While these previous studies were focused on homopolymer brush compositions, copolymer brushes have become a subject of recent research.[61−75] The interest in copolymer brushes has been fueled by the prospect of novel material properties that could be enabled by the deliberate combination of repeat units.[76] For example, random copolymers based on poly(*n*-butyl acrylate-*r*-methyl methacrylate), P(BA-*r*-MMA), were recently proposed to exhibit lock-and-key-type interactions, giving rise to increased material recovery and self-healing ability.[77,78] These findings suggest intriguing opportunities for functional material design. Realizing these opportunities will require an understanding of the role of copolymer brush architecture on the structure and properties of brush particle-based materials. This is because the copolymerization of distinct monomers using techniques such as SI-CRP can result in a variety of distributions of repeat units, such as random or gradient, depending on kinetic constants and reaction conditions.[34]

In this contribution, the effect of BA/MMA composition in grafted random and gradient-type copolymer ligands on the deformation characteristics and thermomechanical properties of particle brush-based hybrid materials was systematically evaluated. A facile method to control copolymer architecture of brush materials based on the variation of the conversion ratio during surface-initiated atom transfer radical polymerization (SI-ATRP) was developed. Subsequently, the thermomechanical properties of random and gradient brush systems were determined and compared with those of the linear copolymer analogues. Depending on the grafting density and composition, gradient polymer architectures exhibited heterogeneous microstructures with distinctively different properties as random copolymer analogues. The results thus highlight the importance of chain architecture as a "control parameter" for the design of functional materials based on copolymer brush particle-based hybrid materials.

RESULTS AND DISCUSSION

We recently reported the synthesis of SiO_2-*g*-PBA-*grad*-PMMA particle brushes with various grafting densities using a semibatch copolymerization activator regenerated by electron transfer (ARGET) surface-initiated atom transfer radical polymerization (SI-ATRP).[47] The deliberate variation of monomer feed ratio and conversion ratio was shown to facilitate the synthesis of gradient and random copolymer brush particle architectures.[79] A detailed analysis of the distribution of various comonomer sequences in the gradient and random copolymers was also recently reported.[79] Here, two series of SiO_2-*g*-PBA-*grad*-PMMA were prepared, i.e. BA-rich region inside ("BA-in") with high (~0.55 chains/nm^2; sample abbreviation: H-G-B_xM_y) and low grafting densities (~0.15 chains/nm^2; sample abbreviation: L-G-B_xM_y) and SiO_2-*g*-PMMA-*grad*-PBA with MMA-rich inside ("MMA-in") and high grafting densities (~0.5 chains/nm^2; sample abbreviation: H-G-M_xB_y) as well as SiO_2-*g*-PBA-*random*-PMMA with high grafting density (~0.5 chains/nm^2; sample abbreviation: H-R-B_xM_y). Note that the sample IDs of brush particle systems are to be read as follows: high/low grafting density (H/L)—random/gradient architecture (R/G)—chemical composition of grafted chains with subscripts, indicating the volume fraction of the respective component. BA-in and

https://doi.org/10.1021/acs.macromol.2c01131
Macromolecules 2022, 55, 8846−8856

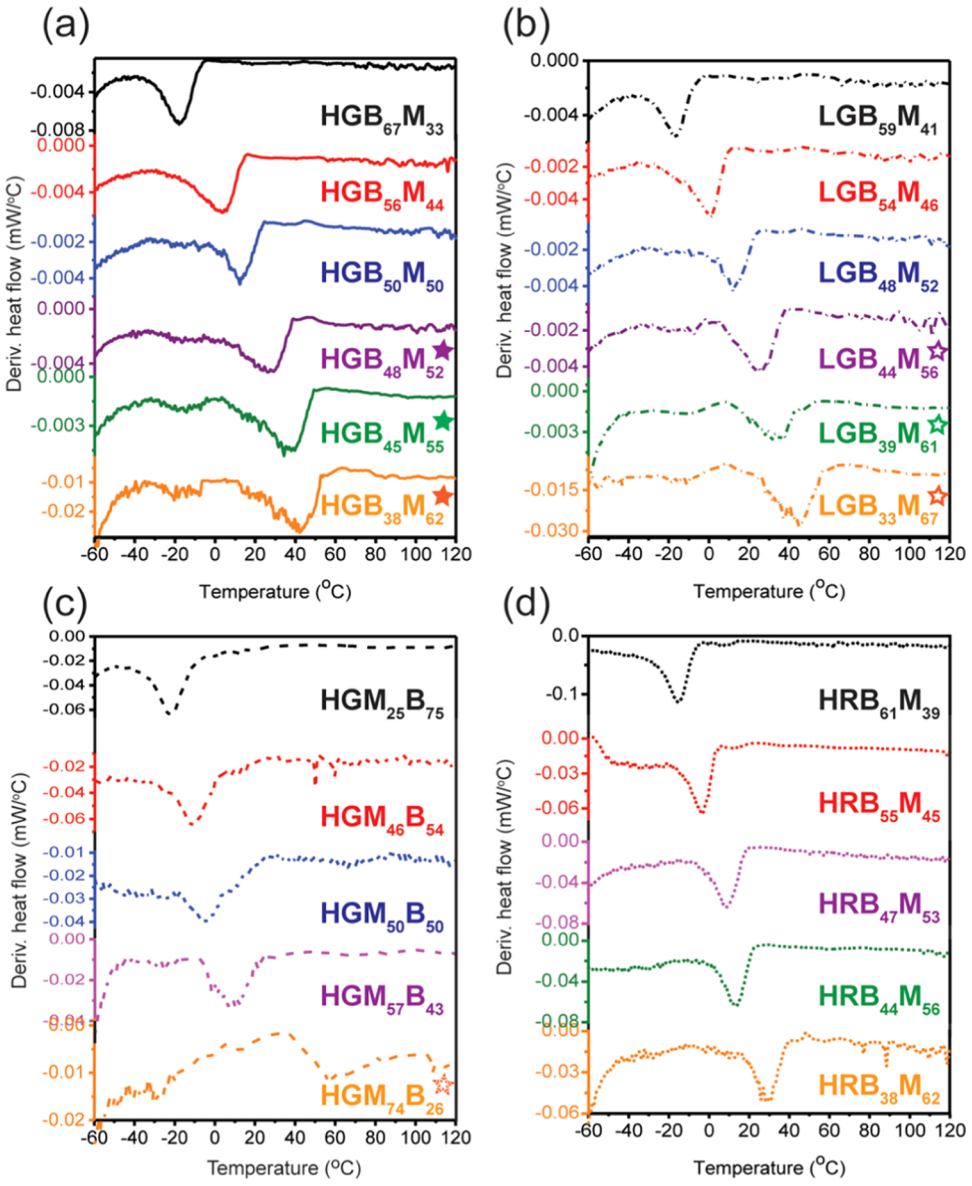

Figure 2. Plots of derivative heat flow vs temperature for (a), (b) BA-rich inside gradient copolymer particle brushes with high (a) and low (b) grafting density; (c) MMA-rich inside gradient copolymer particle brushes with high grafting density as well as densely grafted random copolymer brush systems (d). The stars in the plots highlight the samples for which multiple T_g's can be distinguished in the respective heat flow derivative curves. Sample identification is as follows: panel (a)—solid lines, H-G-$B_{67}M_{33}$: black, H-G-$B_{56}M_{44}$: red, H-G-$B_{50}M_{50}$: blue, H-G-$B_{48}M_{52}$: magenta, H-G-$B_{45}M_{55}$: olive, H-G-$B_{38}M_{62}$: orange; panel (b)—dash-dot lines, L-G-$B_{59}M_{41}$: black, L-G-$B_{54}M_{46}$: red, L-G-$B_{48}M_{52}$: blue, L-G-$B_{44}M_{56}$: magenta, L-G-$B_{39}M_{61}$: olive, L-G-$B_{33}M_{67}$: orange; panel (c)—dash lines, H-G-$M_{25}B_{75}$: black, H-G-$M_{46}B_{54}$: red, H-G-$M_{50}B_{50}$: blue, H-G-$M_{57}B_{43}$: magenta, H-G-$M_{74}B_{26}$: orange; and panel (d)—dot lines, H-R-$B_{61}M_{39}$: black, H-R-$B_{55}M_{45}$: red, H-R-$B_{47}M_{53}$: magenta, H-R-$B_{44}M_{56}$: olive, H-R-$B_{38}M_{62}$: orange. All curves were recorded during the third heating/cooling run at a heating rate of 20 °C/min.

MMA-in gradient brush particles (H-G-B_xM_y, L-G-B_xM_y, H-G-M_xB_y) were synthesized by changing the MMA/BA feeding rate to the ongoing polymerization. The synthetic approaches are illustrated in Scheme 1.

Brush systems were synthesized with varied BA/MMA compositions across the range BA/MMA = 60:40 to 40:60 and with a similar molecular weight. Low grafting densities were realized by mixing a "dummy" initiator (trichlorosilane) in an appropriate ratio with the ATRP initiator during the surface modification step as reported previously.[80] As shown in Table 1, for both H-G-B_xM_y and L-G-B_xM_y gradient copolymer particle brushes, the molecular weight of polymer ligands increased with a higher MMA feeding rate and MMA content in the gradient copolymer ligands, except for samples H-G-$B_{38}M_{62}$ and L-G-$B_{33}M_{67}$.

The drop in molecular weight of samples H-G-$B_{38}M_{62}$/L-G-$B_{33}M_{67}$ could be attributed to the dilution of reactant concentrations by the addition of MMA monomers, which resulted in a decrease in the polymerization rate and thus the molecular weight. To further investigate the effect of sequence and chain architecture on the structure and properties of particle brushes, a series of SiO_2-*g*-P(BA-*r*-MMA) random copolymer particle brush systems was prepared. The conversion of each reaction was limited to below 10% to avoid comonomer feed drift and to achieve a statistically "random" structure. For this condition, previous work has shown that the distribution and sequence of BA/MMA repeat

https://doi.org/10.1021/acs.macromol.2c01131
Macromolecules 2022, 55, 8846−8856

units are determined by the initial monomer concentrations and the reactivity ratios (r_{MMA} = 1.79, r_{BA} = 0.30) (Figure S1).[81] The instantaneous composition of the brush copolymers was calculated from the overall composition, which was monitored during polymerization according to our previous work.[81]

To determine the role of architecture, the composition and molecular weight of random copolymer systems was matched to gradient systems by variation of the initiator content ($[M]_0/[SiO_2\text{-}Br]_0$). The chemical composition, architecture, and microstructure of the copolymer-grafted particle brush systems were systematically characterized as follows: First, the overall PBA/PMMA compositions of the polymer ligands were determined by ^{1}H NMR after etching the silica core with HF aqueous solutions.[47] The corresponding inorganic fractions and grafting density were subsequently obtained by TGA.[47] Subsequently, the morphology and structure of particle brush systems in the solution and solid state were evaluated by dynamic light scattering (DLS) and transmission electron microscopy (TEM). The size of copolymer-grafted brush particles (measured as hydrodynamic radius or by image analysis of electron micrographs) increased with the degree of polymerization following similar trends as homopolymer brush particle analogues (data pertaining to DLS and TEM image analysis curves are shown in Figures S2−S6).[59,60]

To elucidate the effect of copolymer architecture on the microstructure and thermomechanical properties of brush particle materials, the glass transition and mechanical properties were analyzed by differential scanning calorimetry (DSC) and dynamic mechanical analysis (DMA). Figures 1 and 2 depict the heat flow curves (1a−1d) and heat flow derivatives (2a−2d) of gradient BA/MMA copolymer graft brush particle systems with high (Figures 1a,c and 2a,c) and low (Figures 1b and 2b) grafting densities as well as high grafting density random copolymer analogues (Figures 1c and 2c).

Figure 1 reveals several pertinent features that give insight into the role of graft architecture on the structure and properties of brush particle films. First, the figure confirms that the glass-transition temperature (T_g) of all systems increased with the fraction of MMA repeat units. However, for random copolymer brush materials, a single glass transition was observed irrespective of composition (which follows approximately the trend predicted by the Flory−Fox model, Figure S11), and two separate transitions were observed for gradient systems. Splitting into two distinct glass transitions occurred in systems with high (H-G-$B_{48}M_{52}$, H-G-$B_{45}M_{55}$, H-G-$B_{38}M_{62}$; H-G-$M_{74}B_{26}$) and low (L-G-$B_{44}M_{56}$, L-G-$B_{39}M_{61}$, L-G-$B_{33}M_{67}$) grafting densities and with MMA content of approximately 50%. As will be shown below, this "splitting" was a "special feature" of gradient copolymer brush particle films and was not observed for linear gradient copolymers.

Derivative of heat flow curves shown in Figure 2 revealed consistently broader transitions for gradient brush systems as compared to their random brush analogues. The latter featured a breadth of the glass transition (corresponding to the full width at half-maximum of differential heat flow curves) similar to the respective linear copolymer reference systems (Figures S7−S10).[82] For example, for a composition of about 50% MMA, the breadth of the glass transition was $\delta_{T_g\text{H-G-B50M50}}$ = 59 °C, $\delta_{T_g\text{H-G-M50B50}}$ = 51 °C, and $\delta_{T_g\text{L-G-B48M52}}$ = 58 °C for high and low grafting density gradient brushes, whereas for the random analogue, $\delta_{T_g\text{H-R-B47M53}}$ = 32 °C was recorded. The latter value was close to the breadth of the respective linear copolymer analogues with $\delta_{T_g\text{R-B46M54}}$ = 30 °C and $\delta_{T_g\text{G-B45M55}}$ = 51 °C. Likewise, the T_g's of linear random (16 °C) and gradient (18 °C) copolymers were similar to those of the random brush system H-R-$B_{44}M_{56}$ (15 °C) with a comparable composition to the linear analogues (see below).

The trends suggested a (molecularly) uniform microstructure in the case of random copolymer brush particle films. In contrast, the splitting of T_g's in the case of the gradient brush systems was rationalized as an indication of the formation of local heterogeneities viz. BA- and MMA-rich regions. The splitting bears resemblance to the expected behavior of block copolymer-tethered systems; however, the small difference between T_g's suggests the presence of "mixed BA/MMA-rich phases" rather than the formation of compositionally uniform regions that would be expected from a block copolymer-type microphase separation process. As will be shown below, the mechanical behavior of "star-systems" suggests that the regions connect to form a co-continuous morphology. The different (proposed) microstructures for random and gradient brush systems are illustrated in Scheme 2.

Scheme 2. Illustration of Topologically Induced Heterogeneous Microstructure in Films of Gradient Copolymer Particle Brush Systems with Increasing Fraction of MMA Component[a]

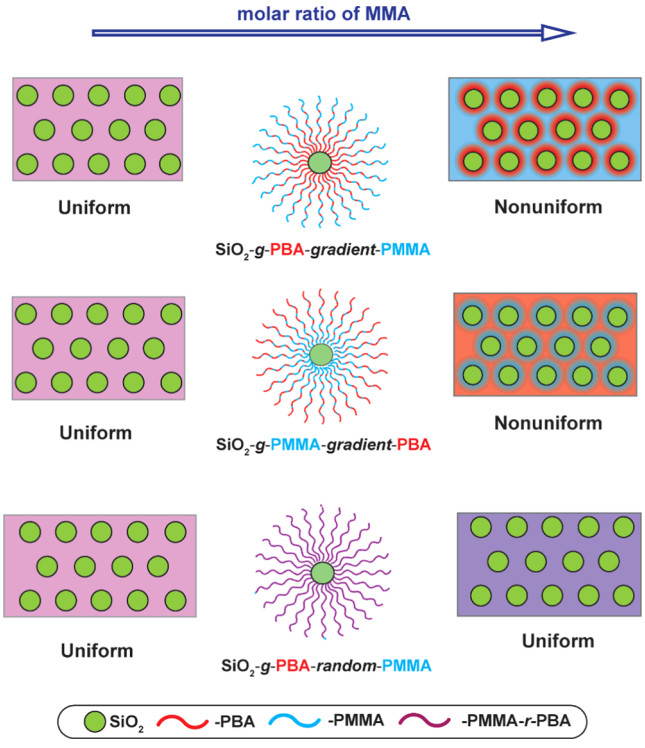

[a]Core−shell structures in nonuniform systems connect to form a co-continuous morphology.

Because the splitting was observed for both high and low grafting densities, we ascribe the heterogeneity formation to the coupling of one chain end to the particle surface rather than the dense or semidilute brush architecture. To further elucidate the implications of microstructure on the properties of random and gradient brush hybrids, the thermomechanical characteristics of all systems were evaluated using uniaxial

https://doi.org/10.1021/acs.macromol.2c01131
Macromolecules 2022, 55, 8846−8856

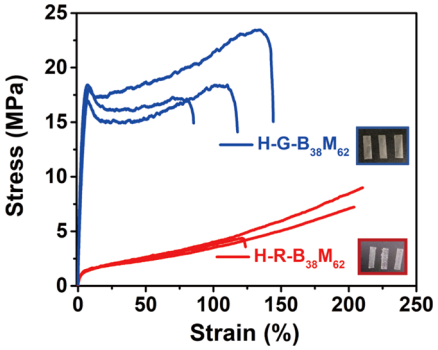

Figure 3. Representative strain−stress curves of high grafting density gradient copolymer particle brushes H-G-$B_{38}M_{62}$ (61.6 mol % MMA, major T_g = 41 °C): blue curves and high grafting density random copolymer particle brushes H-R-$B_{38}M_{62}$ (62.4 mol % MMA, major T_g = 29 °C): red curves (strain rate, 0.005 mm/s; testing temperature, 23 °C). Inset: Photographs of high grafting density gradient/random copolymer particle brushes bulk films; film size: 5 × 15 mm with thickness ∼ 0.1 mm.

stress−strain (Figures 3 and 4) and dynamic mechanical analysis (DMA, Figure 5). Figure 3 displays the room temperature (T = 23 °C) strain−stress curves of H-G-$B_{38}M_{62}$ and H-R-$B_{38}M_{62}$. The bulk films with about 0.1 mm thickness were prepared *via* casting from 40 mg/mL THF solutions. Tensile testing was performed at a constant deformation rate of 0.005 mm/s, and the Young's modulus and toughness were calculated from the incipient slope and by integration of stress−strain curves, respectively. Experiments were repeated three times to evaluate reproducibility. The full set of strain−stress curves is shown in Figures S14−S17 (the low grafting density system L-G-$B_{59}M_{41}$ could not be tested due to the brittleness of the film).

The figure reveals remarkable differences between the respective deformation characteristics, despite the similar composition (x_{MMA} = 61.7 for H-G-$B_{38}M_{62}$ and 62.3 for H-R-$B_{38}M_{62}$) and molar mass ($M_{H\text{-}G\text{-}B38M62}$ = 49.96 kg/mol and $M_{H\text{-}R\text{-}B38M62}$ = 50.04 kg/mol). In particular, the random copolymer system (H-R-$B_{38}M_{62}$, red curves) displayed a strain-to-fracture exceeding 200% uniform plastic deformation and continuous strain hardening. In contrast, deformation of the gradient copolymer system (H-G-$B_{38}M_{62}$, blue curves) displayed a strain-to-fracture of only about 120% along with necking (viz. upper yield point) and strain hardening during drawing. Consistent with its higher T_g, H-G-$B_{38}M_{62}$ displayed a significantly larger Young's modulus ($E_{H\text{-}G\text{-}B38M62}$ = 775 MPa) as compared to H-R-$B_{38}M_{62}$ ($E_{H\text{-}R\text{-}B38M62}$ = 47 MPa). Interestingly, H-G-$B_{38}M_{62}$ also featured a larger toughness (24.2×10^6 J/m^3, determined by integration of stress−strain curves) as compared to the random copolymer brush particle analogue. Figure 4 contrasts Young's moduli and toughness values of all gradient brush systems with high (Figure 4a,c) and low (Figure 4b) grafting densities as well as random architecture (Figure 4d). The figures confirm that the Young's modulus of particle brush systems increased with the fraction of high T_g MMA component (H-G-$B_{67}M_{33}$ → H-G-$B_{38}M_{62}$, H-G-$M_{25}B_{75}$ → H-G-$M_{74}B_{26}$S, and L-G-$B_{54}M_{46}$ → L-G-$B_{33}M_{67}$). However, for the random brush particle films (Figure 4d), the modulus increased continuously with the fraction of MMA, and gradient copolymer brush systems displayed two regimes. In the limit of small MMA fraction, a continuous increase was observed, similar to random linear copolymer analogues. This was followed by a step-like increase of the elastic modulus for gradient samples as the MMA content increased to about 51% (Figure 4a−c). For densely tethered systems, the modulus

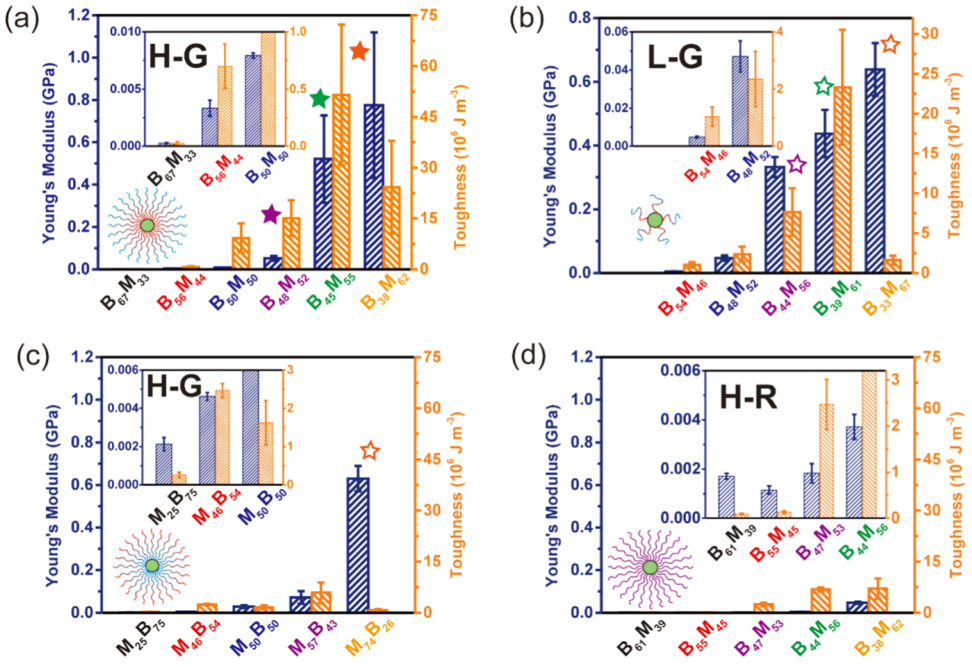

Figure 4. Young's modulus and toughness of copolymer brush particle films determined by uniaxial tension testing. (a, b) BA-in gradient copolymer brush particle solids with high (a) and low (b) grafting densities; (c) MMA-in gradient copolymer particle brushes with high grafting density; (d) densely grafted random copolymer brush systems. The inset shows the Young's modulus and toughness of brush systems on a linear scale to highlight their increase with MMA content. The stars indicate samples featuring a step-like increase of Young's modulus.

https://doi.org/10.1021/acs.macromol.2c01131
Macromolecules 2022, 55, 8846−8856

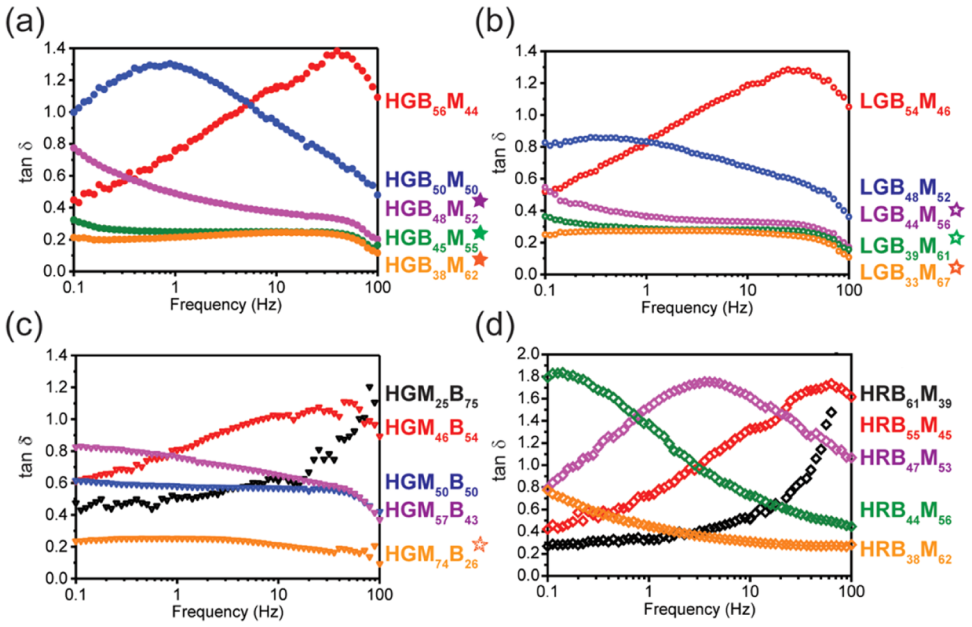

Figure 5. Frequency-dependent loss tangent (tan δ) of brush particle systems at 23 °C across the frequency range of 0.1−100 Hz with 0.1% strain oscillation. (a, b) BA-in gradient copolymer particle brushes with high (a) and low (b) grafting densities; (c) MMA-in gradient copolymer particle brushes with high grafting density; (d) densely grafted random copolymer brush systems (d). Samples are labeled for identification. The stars indicate samples featuring a step-like increase of Young's modulus (see also Figure 4).

increased from 52.0 MPa (H-G-$B_{48}M_{52}$) to 521.0 MPa (H-G-$B_{45}M_{55}$) and 72.4 MPa (H-G-$M_{57}B_{43}$) to 633.0 MPa (H-G-$M_{74}B_{26}$), while for low-density brush particles, the modulus increased from 47.1 MPa (L-G-$B_{48}M_{52}$) to 332.1 MPa (L-G-$B_{44}M_{56}$). Both BA-rich inside and MMA-rich inside gradient brush particles presented a comparable order-of-magnitude increase of the elastic modulus, thus indicating that the formation of heterogeneous regions in gradient brushes, regardless of the gradient chain orientation, resulted in a comparable increase of the materials' cohesive energy density.[59,60] Since the Young's modulus was found to be independent of the direction of stress (not shown here), an isotropic co-continuous morphology was concluded. We note that the fractional increase in modulus for H-G and H-R systems was comparable when normalization with respect to the organic content was performed (see Figure 6 below).

Dynamic mechanical analysis was used to further support the proposed structure formation of gradient brush particle films. Figure 5 shows the loss tangent (tan δ) for gradient brush particles with high (Figure 5a,c) and low (Figure 5b) grafting densities as well as the random copolymer brush analogues (Figure 5d). The figure reveals a similar peak relaxation at ∼40 Hz for H-G-$B_{56}M_{44}$, L-G-$B_{54}M_{46}$, H-G-$M_{46}B_{54}$, and H-R-$B_{55}M_{45}$. The similar relaxation dynamics is consistent with the assumption of a molecularly uniform microstructure at a monomer composition $x_{MMA} \sim 0.51$ (red curves in Figure 5). In contrast, gradient brushes with $x_{MMA} > 0.53$ displayed a significant slowdown of the relaxation frequency as compared to the random brush analogues. For example, the peak relaxation for H-G-$B_{48}M_{52}$, H-G-$M_{57}B_{43}$, and L-G-$B_{44}M_{56}$ is <0.1 Hz and thus outside the experimental resolution, while for the random analogue H-R-$B_{47}M_{53}$, relaxation is observed at ∼3 Hz (purple curves in Figure 5). The slowdown further supported the formation of glassy MMA-rich domains in films of gradient brush particles that "pin" grafted chains. It is interesting to note that the formation

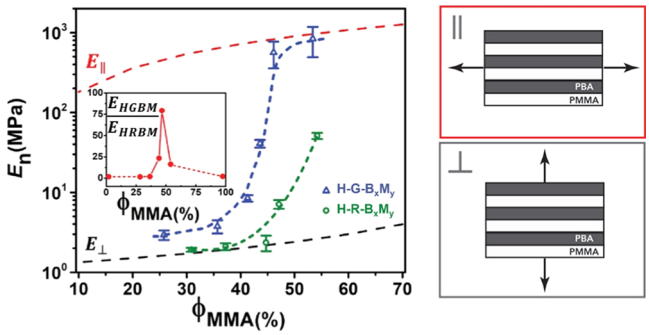

Figure 6. Comparison of normalized Young's moduli of high grafting density gradient/random (HG-B_xM_y/HR-B_xM_y) copolymer particle brush solids vs volume fraction of MMA with effective medium predictions. $E_{||}$ (red dashed curve) represents the upper and $E_\perp$ (gray dashed curve) represents the lower bound corresponding to a layered PBA/PMMA structure with stresses acting in the parallel and transverse direction, respectively. HG-B_xM_y: blue triangles; HR-B_xM_y: green circles. Inset: Modulus ratio of HG-B_xM_y to HR-B_xM_y vs volume fraction of MMA. Schemes indicate reference structures for upper (red) and lower (gray) bound; arrows indicate the direction of stress application.

of an inhomogeneous microstructure in gradient brush systems gave rise to both a step-like increase of Young's modulus and the toughness of films (Figure 4). This indicates that the formation of "hard regions" also introduced new pathways for energy dissipation, which could be useful in designing composite material systems with multiple property enhancements. Since previous work had shown that the elastic properties of brush particle films are determined by ligand dispersion interactions, normalization with respect to the organic fraction could be used to identify the role of brush architecture on the elastic properties.[7,83] Figure 6 displays the normalized Young's moduli $E_n = E_i/f_{org,i}$ of high-density gradient and random brush systems together with the upper

https://doi.org/10.1021/acs.macromol.2c01131
Macromolecules 2022, 55, 8846−8856

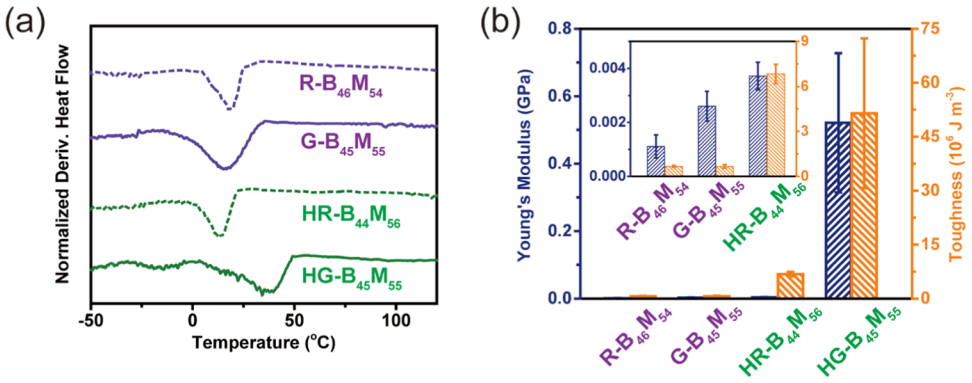

Figure 7. (a) Plot of derivative heat flow vs temperature of linear gradient/random copolymers and gradient/random copolymer particle brush solids with a similar PMMA/PBA composition (BA/MMA = 45:55), (b) Young's modulus and toughness of linear gradient/random copolymers and gradient/random copolymer-grafted SiO_2 particle brushes with the same PMMA/PBA composition (BA/MMA = 45:55).

and lower bounds of a layered PMMA/PBA reference structure ($f_{org,i}$ denotes the fraction of the organic phase in brush system i). Upper ($E_{\parallel}$) and lower ($E_{\perp}$) bounds were calculated according to $E_{\parallel} = E_{PMMA}\phi_{MMA} + E_{PBA}\phi_{BA}$ and $E_{\perp} = (E_{PMMA}E_{PBA})/(\phi_{MMA}E_{PBA} + \phi_{BA}E_{PMMA})$, with ϕ_{MMA} and ϕ_{BA}, denoting the respective volume fraction of MMA and BA. The elastic constants of pure polymer constituents were assumed to be E_{PMMA} = 1800 MPa and E_{PBA} = 1.2 MPa.[84]

Figure 6 reveals that the normalized elastic modulus of BHG brush particle films followed the predicted trend lines for $E_{\perp}$ and $E_{\parallel}$ in the limit of low and high MMA contents, respectively, and displayed a transition between both regimes at $\phi_{crit} \sim 0.45$. The excellent agreement of E_n with the upper bound $E_{\parallel}$ at $\phi_{crit} > 0.45$ suggested the formation of a "co-continuous MMA-rich domain structure" with similar load-bearing capability as the layered reference structure. In contrast, HR brush particle materials were well represented by $E_{\perp}$ in the limit of low MMA content and failed to approach the upper bound over the entire tested compositional range. The maximum slope of E_n is observed at $\phi_{crit} \sim 0.45$, i.e., near the "critical" composition that marks the transition between the stiffness regimes of BHG (see the inset of Figure 6). We thus rationalize this transition as the onset of formation of continuous PMMA-rich regions that store the strain energy upon deformation. Note that this interpretation is also consistent with the splitting of the glass transition into two distinct transitions (Table 1 and Figure 2).

To better understand the role of brush architecture on the formation of a heterogeneous microstructure, the thermal transitions and mechanical properties of copolymer brush particle solids were compared to linear polymer analogues with a similar composition, molecular weight, and chain architecture. A set of linear gradient/random P(BA-*co*-MMA) polymers (G-$B_{45}M_{55}$, R-$B_{46}M_{54}$) with composition PMMA/PBA = 55/45 mol % and molecular weight similar to the grafted polymer chains in H-G-$B_{45}M_{55}$ and H-R-$B_{44}M_{56}$ was prepared using ARGET-ATRP.[85] Figure 7 compares the derivative heat flow curves and the Young's modulus and toughness of linear and brush analogues.

Figure 7a reveals that linear polymers and random brush systems displayed a similar glass transition at T_g = 16 °C (G-$B_{45}M_{55}$), T_g = 18 °C (R-$B_{46}M_{54}$), and T_g = 15 °C (H-R-$B_{44}M_{56}$). The near-identical transition temperatures suggest a "molecularly uniform" microstructure that provides a homogeneous environment for chain relaxation. Interestingly, both random copolymer systems (R-$B_{46}M_{54}$ and H-R-$B_{44}M_{56}$) exhibited a similar breadth of the transition ($\delta_{R\text{-}B46M54}$ = 35 K and $\delta_{H\text{-}R\text{-}B44M56}$ = 34 K), whereas the gradient linear polymer displayed a significantly broader transition with $\delta_{G\text{-}B45M55}$ = 50 K. This confirmed that the gradient architecture introduced some degree of heterogeneity; however, it was not enough to significantly alter the main chain relaxation. This differed from the gradient particle brush system H-G-$B_{45}M_{55}$, which displayed both an increase in the glass-transition temperature and the breadth of the transition ($T_{g,H\text{-}G\text{-}B45M55}$ = 253, 311 K, $\delta_{H\text{-}G\text{-}B45M55}$ = 83 K). As elaborated above, the increase in T_g was rationalized with the formation of co-continuous MMA-rich regions that retard the relaxation of chains (see also Scheme 2) and also contributed to the higher Young's modulus and toughness of H-G-$B_{45}M_{55}$ (Figure 7b). The absence of the slowdown in the G-$B_{45}M_{55}$ reference system indicated that the heterogeneity formation is induced by the defined orientation of chains through surface tethering. This motivates the classification of the heterogeneous microstructure in HG systems as "topologically induced" heterogeneity formation.

CONCLUSIONS

In conclusion, a facile synthetic route toward BA/MMA copolymer brush particles with controlled random and gradient (BA-in/BA-out) architecture was reported. The thermomechanical properties of hybrid materials comprised of brush particle assemblies were sensitive to the architecture of grafted chains. In random copolymer brush systems, the glass-transition temperature followed a similar trend as for linear random copolymer systems, indicating a molecularly uniform microstructure. In contrast, gradient brush particle systems could display, depending on their composition, heterogeneous microstructures that feature an increase in the glass-transition temperature and Young's modulus as well as the toughness of brush particle films. The absence of heterogeneity formation in linear gradient copolymer reference systems highlights the role of geometric constraints that originate from the tethering of chains and the resulting amplification of compositional gradients in brush particle films. We envision that this form of "topology-induced heterogeneity" provides new opportunities for the design of hybrid materials with multiple property enhancements (such as modulus and toughness) that derive from both the chemical

https://doi.org/10.1021/acs.macromol.2c01131
Macromolecules 2022, 55, 8846−8856

composition of copolymer grafts and the microstructure of brush particle assemblies.

■ ASSOCIATED CONTENT

Supporting Information

The Supporting Information is available free of charge at https://pubs.acs.org/doi/10.1021/acs.macromol.2c01131.

Materials; synthetic procedures; characterization procedures (TEM, DLS, TGA, DMA); copolymer composition; electron imaging data of brush particle monolayers; size distribution (DLS); derivative heat flow curves; photographs of mechanical test specimen; and stress−strain and dynamic mechanical characterization data (PDF)

■ AUTHOR INFORMATION

Corresponding Authors

Krzysztof Matyjaszewski − *Department of Chemistry, Carnegie Mellon University, Pittsburgh, Pennsylvania 15213, United States;* orcid.org/0000-0003-1960-3402; Email: km3b@andrew.cmu.edu

Michael R. Bockstaller − *Department of Materials Science & Engineering, Carnegie Mellon University, Pittsburgh, Pennsylvania 15213, United States;* orcid.org/0000-0001-9046-9539; Email: bockstaller@cmu.edu

Authors

Yuqi Zhao − *Department of Materials Science & Engineering, Carnegie Mellon University, Pittsburgh, Pennsylvania 15213, United States;* orcid.org/0000-0002-4438-3635

Zongyu Wang − *Department of Chemistry, Carnegie Mellon University, Pittsburgh, Pennsylvania 15213, United States*

Chenxi Yu − *Department of Materials Science & Engineering, Carnegie Mellon University, Pittsburgh, Pennsylvania 15213, United States*

Hanshu Wu − *Department of Materials Science & Engineering, Carnegie Mellon University, Pittsburgh, Pennsylvania 15213, United States*

Mateusz Olszewski − *Department of Chemistry, Carnegie Mellon University, Pittsburgh, Pennsylvania 15213, United States*

Rongguan Yin − *Department of Chemistry, Carnegie Mellon University, Pittsburgh, Pennsylvania 15213, United States;* orcid.org/0000-0002-8956-3226

Yue Zhai − *Department of Materials Science & Engineering, Carnegie Mellon University, Pittsburgh, Pennsylvania 15213, United States;* orcid.org/0000-0003-0222-7199

Tong Liu − *Department of Chemistry, Carnegie Mellon University, Pittsburgh, Pennsylvania 15213, United States*

Amy Coronado − *Department of Materials Science & Engineering, Carnegie Mellon University, Pittsburgh, Pennsylvania 15213, United States;* orcid.org/0000-0002-6940-6549

Complete contact information is available at: https://pubs.acs.org/10.1021/acs.macromol.2c01131

Author Contributions

[§]Y.Z. and Z.W. contributed equally to this work.

Author Contributions

Y.Z. and Z.W. synthesized materials and performed characterization work. M.O. and R.Y. assisted in the synthesis; C.Y., H.W., Y.Z., and A.C. assisted in the characterization work. M.R.B. and K.M. conceived and organized the project and together with Y.Z. and Z.W. wrote the manuscript.

Notes

The authors declare no competing financial interest.

■ ACKNOWLEDGMENTS

This work was supported by the NSF (CMMI-1663305, DMR 2202747, DMR 2209587, and DMR 1410845) as well as the Scott Institute for Energy Technologies at Carnegie Mellon University. The authors would like to further acknowledge the use of facilities at the Materials Characterization Facility at Carnegie Mellon University under grant MCF-677785.

■ REFERENCES

(1) Boisselier, E.; Diallo, A. K.; Salmon, L.; Ornelas, C.; Ruiz, J.; Astruc, D. Encapsulation and Stabilization of Gold Nanoparticles with "Click" Polyethyleneglycol Dendrimers. *J. Am. Chem. Soc.* **2010**, *132*, 2729−2742.

(2) Peer, D.; Karp, J. M.; Hong, S.; Farokhzad, O. C.; Margalit, R.; Langer, R. Nanocarriers as an emerging platform for cancer therapy. *Nat. Nanotechnol.* **2007**, *2*, 751−760.

(3) Zhen, Z.; Tang, W.; Wang, M.; Zhou, S.; Wang, H.; Wu, Z.; Hao, Z.; Li, Z.; Liu, L.; Xie, J. Protein Nanocage Mediated Fibroblast-Activation Protein Targeted Photoimmunotherapy To Enhance Cytotoxic T Cell Infiltration and Tumor Control. *Nano Lett.* **2017**, *17*, 862−869.

(4) Mahoney, C.; Hui, C. M.; Majumdar, S.; Wang, Z.; Malen, J. A.; Tchoul, M.; Matyjaszewski, K.; Bockstaller, M. R. Enhancing thermal transport in nanocomposites by polymer-graft modification of particle fillers. *Polymer* **2016**, *93*, 72−77.

(5) Cang, Y.; Lee, J.; Wang, Z.; Yan, J.; Matyjaszewski, K.; Bockstaller, M. R.; Fytas, G. Transparent Hybrid Opals with Unexpected Strong Resonance-Enhanced Photothermal Energy Conversion. *Adv. Mater.* **2021**, *33*, No. 2004732.

(6) Alonso-Redondo, E.; Schmitt, M.; Urbach, Z.; Hui, C. M.; Sainidou, R.; Rembert, P.; Matyjaszewski, K.; Bockstaller, M. R.; Fytas, G. A new class of tunable hypersonic phononic crystals based on polymer-tethered colloids. *Nat. Commun.* **2015**, *6*, No. 8309.

(7) Lee, J.; Wang, Z.; Zhang, J.; Yan, J.; Deng, T.; Zhao, Y.; Matyjaszewski, K.; Bockstaller, M. R. Molecular Parameters Governing the Elastic Properties of Brush Particle Films. *Macromolecules* **2020**, *53*, 1502−1513.

(8) Kumar, S. K.; Benicewicz, B. C.; Vaia, R. A.; Winey, K. I. 50th Anniversary Perspective: Are Polymer Nanocomposites Practical for Applications? *Macromolecules* **2017**, *50*, 714−731.

(9) Moll, J. F.; Akcora, P.; Rungta, A.; Gong, S.; Colby, R. H.; Benicewicz, B. C.; Kumar, S. K. Mechanical Reinforcement in Polymer Melts Filled with Polymer Grafted Nanoparticles. *Macromolecules* **2011**, *44*, 7473−7477.

(10) Zheng, Y.; Wang, L.; Lu, L.; Wang, Q.; Benicewicz, B. C. pH and Thermal Dual-Responsive Nanoparticles for Controlled Drug Delivery with High Loading Content. *ACS Omega* **2017**, *2*, 3399−3405.

(11) Tao, P.; Li, Y.; Rungta, A.; Viswanath, A.; Gao, J.; Benicewicz, B. C.; Siegel, R. W.; Schadler, L. S. TiO2 nanocomposites with high refractive index and transparency. *J. Mater. Chem.* **2011**, *21*, 18623−18629.

(12) Bilchak, C. R.; Jhalaria, M.; Huang, Y.; Abbas, Z.; Midya, J.; Benedetti, F. M.; Parisi, D.; Egger, W.; Dickmann, M.; Minelli, M.; Doghieri, F.; Nikoubashman, A.; Durning, C. J.; Vlassopoulos, D.; Jestin, J.; Smith, Z. P.; Benicewicz, B. C.; Rubinstein, M.; Leibler, L.; Kumar, S. K. Tuning Selectivities in Gas Separation Membranes Based on Polymer-Grafted Nanoparticles. *ACS Nano* **2020**, *14*, 17174−17183.

(13) Hakem, I. F.; Leech, A. M.; Johnson, J. D.; Donahue, S. J.; Walker, J. P.; Bockstaller, M. R. Understanding Ligand Distributions

in Modified Particle and Particlelike Systems. *J. Am. Chem. Soc.* **2010**, *132*, 16593−16598.
(14) Qiao, Y.; Islam, M. S.; Wang, L.; Yan, Y.; Zhang, J.; Benicewicz, B. C.; Ploehn, H. J.; Tang, C. Thiophene Polymer-Grafted Barium Titanate Nanoparticles toward Nanodielectric Composites. *Chem. Mater.* **2014**, *26*, 5319−5326.
(15) Kim, P.; Doss, N. M.; Tillotson, J. P.; Hotchkiss, P. J.; Pan, M.-J.; Marder, S. R.; Li, J.; Calame, J. P.; Perry, J. W. High Energy Density Nanocomposites Based on Surface-Modified BaTiO3 and a Ferroelectric Polymer. *ACS Nano* **2009**, *3*, 2581−2592.
(16) Yokoyama, R.; Suzuki, S.; Shirai, K.; Yamauchi, T.; Tsubokawa, N.; Tsuchimochi, M. Preparation and properties of biocompatible polymer-grafted silica nanoparticle. *Eur. Polym. J.* **2006**, *42*, 3221−3229.
(17) Bilchak, C. R.; Huang, Y.; Benicewicz, B. C.; Durning, C. J.; Kumar, S. K. High-Frequency Mechanical Behavior of Pure Polymer-Grafted Nanoparticle Constructs. *ACS Macro Lett.* **2019**, *8*, 294−298.
(18) Tchoul, M. N.; Fillery, S. P.; Koerner, H.; Drummy, L. F.; Oyerokun, F. T.; Mirau, P. A.; Durstock, M. F.; Vaia, R. A. Assemblies of Titanium Dioxide-Polystyrene Hybrid Nanoparticles for Dielectric Applications. *Chem. Mater.* **2010**, *22*, 1749−1759.
(19) Mbanga, B. L.; Iyer, B. V. S.; Yashin, V. V.; Balazs, A. C. Tuning the Mechanical Properties of Polymer-Grafted Nanoparticle Networks through the Use of Biomimetic Catch Bonds. *Macromolecules* **2016**, *49*, 1353−1361.
(20) Hansoge, N. K.; Huang, T.; Sinko, R.; Xia, W.; Chen, W.; Keten, S. Materials by Design for Stiff and Tough Hairy Nanoparticle Assemblies. *ACS Nano* **2018**, *12*, 7946−7958.
(21) Fernandes, N. J.; Koerner, H.; Giannelis, E. P.; Vaia, R. A. Hairy nanoparticle assemblies as one-component functional polymer nanocomposites: opportunities and challenges. *MRS Commun.* **2013**, *3*, 13−29.
(22) Zhang; Horsch, M. A.; Lamm, M. H.; Glotzer, S. C. Tethered Nano Building Blocks: Toward a Conceptual Framework for Nanoparticle Self-Assembly. *Nano Lett.* **2003**, *3*, 1341−1346.
(23) Zou, H.; Wu, S.; Shen, J. Polymer/Silica Nanocomposites: Preparation, Characterization, Properties, and Applications. *Chem. Rev.* **2008**, *108*, 3893−3957.
(24) Adibnia, V.; Mirbagheri, M.; Faivre, J.; Robert, J.; Lee, J.; Matyjaszewski, K.; Lee, D. W.; Banquy, X. Bioinspired polymers for lubrication and wear resistance. *Prog. Polym. Sci.* **2020**, *110*, No. 101298.
(25) Abbas, Z. M.; Tawfilas, M.; Khani, M. M.; Golian, K.; Marsh, Z. M.; Jhalaria, M.; Simonutti, R.; Stefik, M.; Kumar, S. K.; Benicewicz, B. C. Reinforcement of polychloroprene by grafted silica nanoparticles. *Polymer* **2019**, *171*, 96−105.
(26) Midya, J.; Rubinstein, M.; Kumar, S. K.; Nikoubashman, A. Structure of Polymer-Grafted Nanoparticle Melts. *ACS Nano* **2020**, *14*, 15505−15516.
(27) Alkhodairi, H.; Russell, S. T.; Pribyl, J.; Benicewicz, B. C.; Kumar, S. K. Compatibilizing Immiscible Polymer Blends with Sparsely Grafted Nanoparticles. *Macromolecules* **2020**, *53*, 10330−10338.
(28) Chen, S. H.; Souna, A. J.; Stranick, S. J.; Jhalaria, M.; Kumar, S. K.; Soles, C. L.; Chan, E. P. Controlling toughness of polymer-grafted nanoparticle composites for impact mitigation. *Soft Matter* **2022**, *18*, 256−261.
(29) Hore, M. J. A. Polymers on nanoparticles: structure & dynamics. *Soft Matter* **2019**, *15*, 1120−1134.
(30) Wijmans, C. M.; Zhulina, E. B. Polymer brushes at curved surfaces. *Macromolecules* **1993**, *26*, 7214−7224.
(31) Williams, G. A.; Ishige, R.; Cromwell, O. R.; Chung, J.; Takahara, A.; Guan, Z. Mechanically Robust and Self-Healable Superlattice Nanocomposites by Self-Assembly of Single-Component "Sticky" Polymer-Grafted Nanoparticles. *Adv. Mater.* **2015**, *27*, 3934−3941.
(32) Tsujii, Y.; Ohno, K.; Yamamoto, S.; Goto, A.; Fukuda, T. Structure and Properties of High-Density Polymer Brushes Prepared by Surface-Initiated Living Radical Polymerization. In *Surface-Initiated Polymerization I*, Jordan, R., Ed.; Springer: Berlin, Heidelberg, 2006; pp 1−45.
(33) Barbey, R.; Lavanant, L.; Paripovic, D.; Schüwer, N.; Sugnaux, C.; Tugulu, S.; Klok, H.-A. Polymer Brushes via Surface-Initiated Controlled Radical Polymerization: Synthesis, Characterization, Properties, and Applications. *Chem. Rev.* **2009**, *109*, 5437−5527.
(34) Hui, C. M.; Pietrasik, J.; Schmitt, M.; Mahoney, C.; Choi, J.; Bockstaller, M. R.; Matyjaszewski, K. Surface-Initiated Polymerization as an Enabling Tool for Multifunctional (Nano-)Engineered Hybrid Materials. *Chem. Mater.* **2014**, *26*, 745−762.
(35) Yan, J.; Bockstaller, M. R.; Matyjaszewski, K. Brush-modified materials: Control of molecular architecture, assembly behavior, properties and applications. *Prog. Polym. Sci.* **2020**, *100*, No. 101180.
(36) Ethier, J. G.; Hall, L. M. Structure and Entanglement Network of Model Polymer-Grafted Nanoparticle Monolayers. *Macromolecules* **2018**, *51*, 9878−9889.
(37) Jancar, J.; Douglas, J. F.; Starr, F. W.; Kumar, S. K.; Cassagnau, P.; Lesser, A. J.; Sternstein, S. S.; Buehler, M. J. Current issues in research on structure−property relationships in polymer nanocomposites. *Polymer* **2010**, *51*, 3321−3343.
(38) Kumar, S. K.; Krishnamoorti, R. Nanocomposites: structure, phase behavior, and properties. *Annu. Rev. Chem. Biomol. Eng.* **2010**, *1*, 37−58.
(39) Vaia, R. A.; Maguire, J. F. Polymer Nanocomposites with Prescribed Morphology: Going beyond Nanoparticle-Filled Polymers. *Chem. Mater.* **2007**, *19*, 2736−2751.
(40) Jiao, Y.; Tibbits, A.; Gillman, A.; Hsiao, M.-S.; Buskohl, P.; Drummy, L. F.; Vaia, R. A. Deformation Behavior of Polystyrene-Grafted Nanoparticle Assemblies with Low Grafting Density. *Macromolecules* **2018**, *51*, 7257−7265.
(41) Altorbaq, A. S.; Jimenez, A. M.; Pribyl, J.; Benicewicz, B.; Müller, A. J.; Kumar, S. K. Polymer Spherulitic Growth Kinetics Mediated by Nanoparticle Assemblies. *Macromolecules* **2021**, *54*, 1063−1072.
(42) Liu, C.-H.; Pan, C.-Y. Grafting polystyrene onto silica nanoparticles via RAFT polymerization. *Polymer* **2007**, *48*, 3679−3685.
(43) Lenart, W. R.; Hore, M. J. A. Structure−property relationships of polymer-grafted nanospheres for designing advanced nanocomposites. *Nano-Struct. Nano-Objects* **2018**, *16*, 428−440.
(44) Pribyl, J.; Benicewicz, B. C. Surface and Particle Modification via RAFT Polymerization: An Update. *RAFT Polym.* **2021**, 1017−1049.
(45) Choi, J.; Dong, H.; Matyjaszewski, K.; Bockstaller, M. R. Flexible Particle Array Structures by Controlling Polymer Graft Architecture. *J. Am. Chem. Soc.* **2010**, *132*, 12537−12539.
(46) Vlassopoulos, D.; Fytas, G. From Polymers to Colloids: Engineering the Dynamic Properties of Hairy Particles. In *High Solid Dispersions*, Cloitre, M., Ed.; Springer: Berlin, Heidelberg, 2010; pp 1−54.
(47) Wang, Z.; Liu, T.; Zhao, Y.; Lee, J.; Wei, Q.; Yan, J.; Li, S.; Olszewski, M.; Yin, R.; Zhai, Y.; Bockstaller, M. R.; Matyjaszewski, K. Synthesis of Gradient Copolymer Grafted Particle Brushes by ATRP. *Macromolecules* **2019**, *52*, 9466−9475.
(48) Dervaux, B.; Junkers, T.; Barner-Kowollik, C.; Du Prez, F. E. Continuous ATRP Synthesis of Block-Like Copolymers via Column Reactors: Design and Validation of a Kinetic Model. *Macromol. React. Eng.* **2009**, *3*, 529−538.
(49) Mok, M. M.; Kim, J.; Torkelson, J. M. Gradient copolymers with broad glass transition temperature regions: Design of purely interphase compositions for damping applications. *J. Polym. Sci., Part B: Polym. Phys.* **2008**, *46*, 48−58.
(50) Kim, J.; Mok, M. M.; Sandoval, R. W.; Woo, D. J.; Torkelson, J. M. Uniquely Broad Glass Transition Temperatures of Gradient Copolymers Relative to Random and Block Copolymers Containing Repulsive Comonomers. *Macromolecules* **2006**, *39*, 6152−6160.
(51) Wong, C. L. H.; Kim, J.; Roth, C. B.; Torkelson, J. M. Comparison of Critical Micelle Concentrations of Gradient Copolymer and Block Copolymer in Homopolymer: Novel

https://doi.org/10.1021/acs.macromol.2c01131
Macromolecules 2022, 55, 8846−8856

Characterization by Intrinsic Fluorescence. *Macromolecules* **2007**, *40*, 5631−5633.
(52) Dettmer, C. M.; Gray, M. K.; Torkelson, J. M.; Nguyen, S. T. Synthesis and Functionalization of ROMP-Based Gradient Copolymers of 5-Substituted Norbornenes. *Macromolecules* **2004**, *37*, 5504−5512.
(53) Cheng, C.-H.; Masuda, S.; Nozaki, S.; Nagano, C.; Hirai, T.; Kojio, K.; Takahara, A. Fabrication and Deformation of Mechanochromic Nanocomposite Elastomers Based on Rubbery and Glassy Block Copolymer-Grafted Silica Nanoparticles. *Macromolecules* **2020**, *53*, 4541−4551.
(54) Matyjaszewski, K.; Ziegler, M. J.; Arehart, S. V.; Greszta, D.; Pakula, T. Gradient copolymers by atom transfer radical copolymerization. *J. Phys. Org. Chem.* **2000**, *13*, 775−786.
(55) Davis, K. A.; Matyjaszewski, K. *Statistical, Gradient, Block and Graft Copolymers by Controlled/Living Radical Polymerizations*; Springer, 2002.
(56) Matyjaszewski, K.; Tsarevsky, N. V. Macromolecular Engineering by Atom Transfer Radical Polymerization. *J. Am. Chem. Soc.* **2014**, *136*, 6513−6533.
(57) Matyjaszewski, K.; Tsarevsky, N. V. Nanostructured functional materials prepared by atom transfer radical polymerization. *Nat. Chem.* **2009**, *1*, 276−288.
(58) Voudouris, P.; Choi, J.; Dong, H.; Bockstaller, M. R.; Matyjaszewski, K.; Fytas, G. Effect of Shell Architecture on the Static and Dynamic Properties of Polymer-Coated Particles in Solution. *Macromolecules* **2009**, *42*, 2721−2728.
(59) Choi, J.; Hui, C. M.; Pietrasik, J.; Dong, H.; Matyjaszewski, K.; Bockstaller, M. R. Toughening fragile matter: mechanical properties of particle solids assembled from polymer-grafted hybrid particles synthesized by ATRP. *Soft Matter* **2012**, *8*, 4072−4082.
(60) Schmitt, M.; Choi, J.; Min Hui, C.; Chen, B.; Korkmaz, E.; Yan, J.; Margel, S.; Burak Ozdoganlar, O.; Matyjaszewski, K.; Bockstaller, M. R. Processing fragile matter: effect of polymer graft modification on the mechanical properties and processibility of (nano-) particulate solids. *Soft Matter* **2016**, *12*, 3527−3537.
(61) Wang, Z.; Lee, J.; Wang, Z.; Zhao, Y.; Yan, J.; Lin, Y.; Li, S.; Liu, T.; Olszewski, M.; Pietrasik, J.; Bockstaller, M. R.; Matyjaszewski, K. Tunable Assembly of Block Copolymer Tethered Particle Brushes by Surface-Initiated Atom Transfer Radical Polymerization. *ACS Macro Lett.* **2020**, *9*, 806−812.
(62) Laub, C. F.; Koberstein, J. T. Effect of Brush Polydispersity on the Interphase between End-Grafted Brushes and Polymeric Matrixes. *Macromolecules* **1994**, *27*, 5016−5023.
(63) Kumar, S. K.; Jouault, N.; Benicewicz, B.; Neely, T. Nanocomposites with Polymer Grafted Nanoparticles. *Macromolecules* **2013**, *46*, 3199−3214.
(64) Gao, J.; Li, J.; Benicewicz, B. C.; Zhao, S.; Hillborg, H.; Schadler, L. S. The Mechanical Properties of Epoxy Composites Filled with Rubbery Copolymer Grafted SiO2. *Polymers* **2012**, *4*, 187−210.
(65) Gupta, S.; Chokshi, P. Diblock copolymer templated self-assembly of grafted nanoparticles under circular pore confinement. *Soft Matter* **2020**, *16*, 3522−3535.
(66) He, L.; Theato, P. Collagen and collagen mimetic peptide conjugates in polymer science. *Eur. Polym. J.* **2013**, *49*, 2986−2997.
(67) Li, D.; Cui, Y.; Wang, K.; He, Q.; Yan, X.; Li, J. Thermosensitive Nanostructures Comprising Gold Nanoparticles Grafted with Block Copolymers. *Adv. Funct. Mater.* **2007**, *17*, 3134−3140.
(68) Lin, Y.; Böker, A.; He, J.; Sill, K.; Xiang, H.; Abetz, C.; Li, X.; Wang, J.; Emrick, T.; Long, S.; Wang, Q.; Balazs, A.; Russell, T. P. Self-directed self-assembly of nanoparticle/copolymer mixtures. *Nature* **2005**, *434*, 55−59.
(69) Tang, S.; Horton, J. M.; Zhao, B.; Zhu, L. Self-organization of homopolymer brush- and mixed homopolymer brush-grafted silica nanoparticles in block copolymers and polymer blends. *Polymer* **2016**, *90*, 9−17.
(70) Sarkar, B. R.; Alexandridis, P. Block copolymer-nanoparticle composites: Structure, functional properties, and processing. *Prog. Polym. Sci.* **2015**, *40*, 33−62.
(71) Fernández-de-Alba, C.; Jimenez, A. M.; Abbasi, M.; Kumar, S. K.; Saalwächter, K.; Baeza, G. P. On the Immobilized Polymer Fraction in Attractive Nanocomposites: Tg Gradient versus Interfacial Layer. *Macromolecules* **2021**, *54*, 10289−10299.
(72) Xu, C.; Ohno, K.; Ladmiral, V.; Composto, R. J. Dispersion of polymer-grafted magnetic nanoparticles in homopolymers and block copolymers. *Polymer* **2008**, *49*, 3568−3577.
(73) Maguire, S. M.; Boyle, M. J.; Bilchak, C. R.; Demaree, J. D.; Keller, A. W.; Krook, N. M.; Ohno, K.; Kagan, C. R.; Murray, C. B.; Rannou, P.; Composto, R. J. Grafted Nanoparticle Surface Wetting during Phase Separation in Polymer Nanocomposite Films. *ACS Appl. Mater. Interfaces* **2021**, *13*, 37628−37637.
(74) Hore, M. J. A.; Ford, J.; Ohno, K.; Composto, R. J.; Hammouda, B. Direct Measurements of Polymer Brush Conformation Using Small-Angle Neutron Scattering (SANS) from Highly Grafted Iron Oxide Nanoparticles in Homopolymer Melts. *Macromolecules* **2013**, *46*, 9341−9348.
(75) Lee, P. W.; Isarov, S. A.; Wallat, J. D.; Molugu, S. K.; Shukla, S.; Sun, J. E. P.; Zhang, J.; Zheng, Y.; Lucius Dougherty, M.; Konkolewicz, D.; Stewart, P. L.; Steinmetz, N. F.; Hore, M. J. A.; Pokorski, J. K. Polymer Structure and Conformation Alter the Antigenicity of Virus-like Particle−Polymer Conjugates. *J. Am. Chem. Soc.* **2017**, *139*, 3312−3315.
(76) Huang, Y.; Zheng, Y.; Sarkar, A.; Xu, Y.; Stefik, M.; Benicewicz, B. C. Matrix-Free Polymer Nanocomposite Thermoplastic Elastomers. *Macromolecules* **2017**, *50*, 4742−4753.
(77) Wang, S.; Urban, M. W. Self-healing polymers. *Nat. Rev. Mater.* **2020**, *5*, 562−583.
(78) Yang, Y.; Urban, M. W. Self-healing polymeric materials. *Chem. Soc. Rev.* **2013**, *42*, 7446−7467.
(79) Sosnowski, S.; Szymanski, R.; Lorandi, F.; Olszewski, M.; Sobieski, J.; Yin, R.; Bockstaller, M. R.; Matyjaszewski, K. Distribution of Alternating Sequences in Methyl Methacrylate/n-Butyl Acrylate Copolymers Prepared by Atom Transfer Radical Polymerization. *Macromolecules* **2021**, *54*, 9837−9849.
(80) Wang, Z.; Liu, T.; Lin, K. C.; Li, S.; Yan, J.; Olszewski, M.; Sobieski, J.; Pietrasik, J.; Bockstaller, M. R.; Matyjaszewski, K. Synthesis of Ultra-high Molecular Weight SiO2-g-PMMA Particle Brushes. *J. Inorg. Organomet. Polym. Mater.* **2019**, *30*, 174−181.
(81) Roos, S. G.; Müller, A. H. E.; Matyjaszewski, K. Copolymerization of n-Butyl Acrylate with Methyl Methacrylate and PMMA Macromonomers: Comparison of Reactivity Ratios in Conventional and Atom Transfer Radical Copolymerization. *Macromolecules* **1999**, *32*, 8331−8335.
(82) Fox, T. G.; Flory, P. J. Second-Order Transition Temperatures and Related Properties of Polystyrene. I. Influence of Molecular Weight. *J. Appl. Phys.* **1950**, *21*, 581−591.
(83) Podsiadlo, P.; Krylova, G.; Lee, B.; Critchley, K.; Gosztola, D. J.; Talapin, D. V.; Ashby, P. D.; Shevchenko, E. V. The Role of Order, Nanocrystal Size, and Capping Ligands in the Collective Mechanical Response of Three-Dimensional Nanocrystal Solids. *J. Am. Chem. Soc.* **2010**, *132*, 8953−8960.
(84) Humlicek, J. Data Analysis for Nanomaterials: Effective Medium Approximation, Its Limits and Implementations. In *Ellipsometry at the Nanoscale*; Losurdo, M.; Hingerl, K., Eds.; Springer: Berlin, Heidelberg, 2013; pp 145−178.
(85) Tanaka, K.; Matyjaszewski, K. Controlled Copolymerization of n-Butyl Acrylate with Nonpolar 1-Alkenes Using Activators Regenerated by Electron Transfer for Atom-Transfer Radical Polymerization. *Macromolecules* **2007**, *40*, 5255−5260.

https://doi.org/10.1021/acs.macromol.2c01131
Macromolecules 2022, 55, 8846−8856